

Cross-Resolution Attention Network for High-Resolution PM_{2.5} Prediction

Ammar Kheder^{2,3*} Helmi Toropainen^{1,3} Wenqing Peng^{1,3} Samuel Antão⁴ Zhi-Song Liu^{2,3,**} Michael Boy^{1,2,3}

¹Institute for Atmospheric and Earth System Research, University of Helsinki, P.O. Box 64, Helsinki 00014, Finland

²Department of Computational Engineering, LUT University, Finland

³Atmospheric Modelling Centre Lahti (AMC-Lahti), Finland

⁴Advanced Micro Devices (AMD), Munich, Germany

Abstract

Vision Transformers have achieved remarkable success in spatio-temporal prediction, but their scalability remains limited for ultra-high-resolution, continent-scale domains required in real-world environmental monitoring. A single European air-quality map at 1 km resolution comprises 29 million pixels, far beyond the limits of naive self-attention. We introduce **CRAN-PM**, a dual-branch Vision Transformer that leverages cross-resolution attention to efficiently fuse global meteorological data (25 km) with local high-resolution PM_{2.5} at the current time (1 km). Instead of including physically driven factors like temperature and topography as input, we further introduce elevation-aware self-attention and wind-guided cross-attention to force the network to learn physically consistent feature representations for PM_{2.5} forecasting. CRAN-PM is fully trainable and memory-efficient, generating the complete 29-million-pixel European map in 1.8 seconds on a single GPU. Evaluated on daily PM_{2.5} forecasting throughout Europe in 2022 (362 days, 2,971 European Environment Agency (EEA) stations), it reduces RMSE by 4.7% at T+1 and 10.7% at T+3 compared to the best single-scale baseline, while reducing bias in complex terrain by 36%.

Keywords: PM_{2.5}, Air Pollution Prediction, Vision Transformers, Cross-Resolution Attention, Physics-Guided Deep Learning

Code: https://github.com/AmmarKheder/cran_pm

1 Introduction

Vision Transformers [10] have transformed image and video processing for spatio-temporal analysis, with models such as Swin Transformer [21], VPTR [36], ViViT [1], Earthformer [12], and ClimaX [24] achieving state-of-the-art results across video prediction, weather forecasting, and remote sensing. Yet all of these methods share a fundamental limitation: they operate at a single, fixed spatial resolution. When the target domain is large and the required resolution is fine, the token count explodes and the model becomes intractable. This is not merely an engineering inconvenience; it is a structural barrier preventing Vision Transformers from addressing real-world problems requiring both ultra-high resolution and long-range spatial context.

Our goal is to design a PM_{2.5} forecasting model that takes the current observation to predict future evolution at fine resolution (1 km × 1 km). However, a European map at this resolution is approximately 4000 × 8000 pixels, yielding ~115,000 tokens when tokenized, far exceeding memory limits for standard self-attention. Independent tiling discards

*Corresponding: ammar.kheder@lut.fi

**Corresponding: zhisong.liu@lut.fi

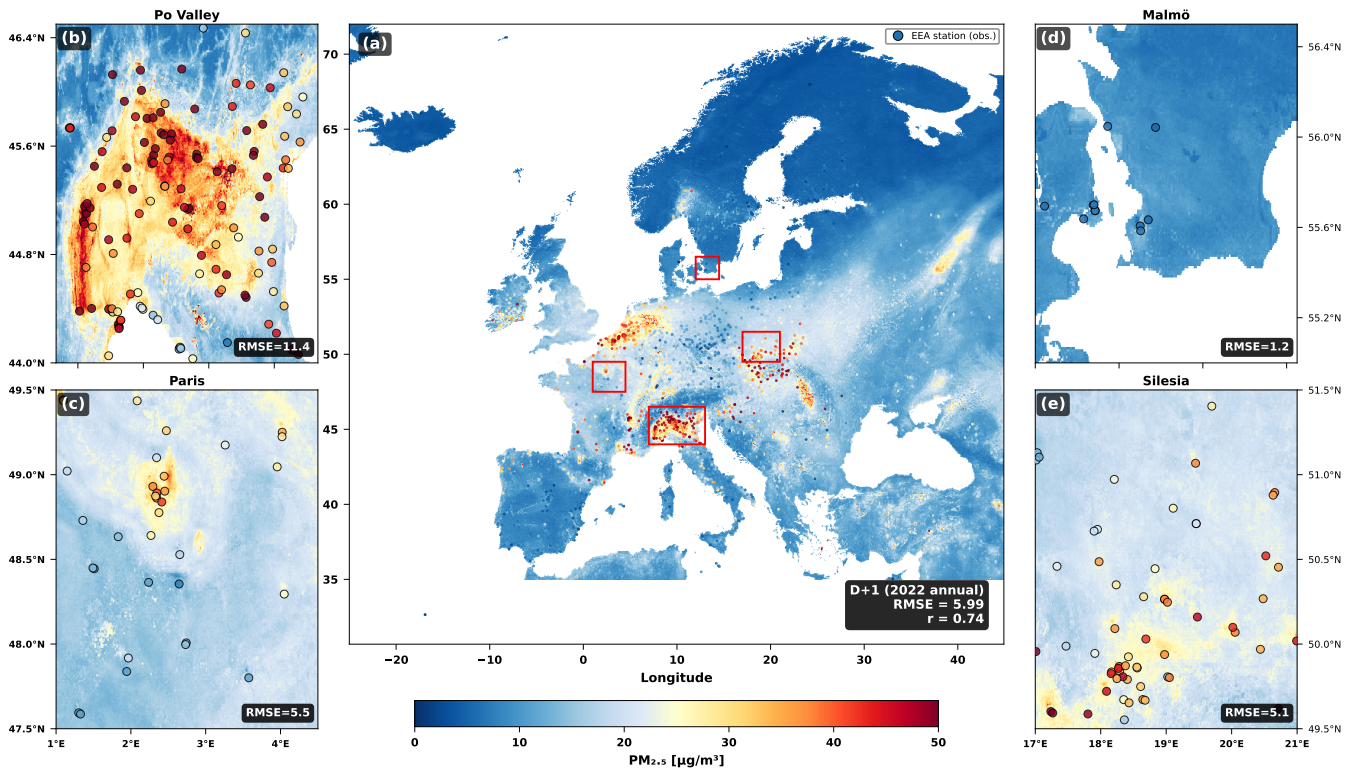


Figure 1: CRAN-PM predicts daily $PM_{2.5}$ at 1 km resolution across Europe. (a) Full European prediction for January 25, 2022 (T+1 horizon). Red rectangles indicate zoom regions. (b–e) Regional details for Po Valley, Paris, Malmö, and Silesia. Colored circles represent independent EEA ground station measurements. Annual T+1 performance: $RMSE = 5.99 \mu\text{g}/\text{m}^3$, $r = 0.74$.

the large-scale meteorological context (advection, boundary-layer stability) driving local pollution. Existing methods either maintain global consistency at coarse resolutions ($\geq 10\text{--}40\text{ km}$) [3, 4, 13, 16, 17], or provide retrospective 1 km estimates without forecasting capabilities [34]. The central question is: *how can a Vision Transformer handle ultra-high-resolution forecasting over continental domains without losing global physical context?*

We introduce **CRAN-PM** (Fig. 2), a dual-branch Vision Transformer designed for scalable, high-resolution air-quality forecasting. A **global branch** encodes large-scale meteorology over the full domain at 25 km resolution, while a **local branch** processes overlapping 1 km tiles on the current high-resolution $PM_{2.5}$ data. The branches communicate via **cross-resolution attention**, enabling the local branch to query the global branch for long-range context. This reduces per-tile memory to under 2 GB while preserving physically meaningful interactions. We further propose elevation-aware self-attention bias and a wind-guided cross-attention bias as soft physical constraints.

Our contributions are:

- Existing methods either upsample coarse meteorology or downsample fine-resolution $PM_{2.5}$ to enforce uniform inputs, discarding spatial detail or introducing interpolation artefacts. We instead propose a dual-branch Vision Transformer that processes global meteorological fields and local $PM_{2.5}$ patches at their native resolutions, bridging them via cross-attention. This lets the model learn which atmospheric drivers most influence each local region without any resolution compromise.
- We incorporate elevation and wind-field priors as soft additive biases in the attention, grounding the model in known physical transport mechanisms. These priors require no additional parameters and improve accuracy at complex-terrain stations where data-driven baselines systematically fail.

- To our knowledge, this is the first deep-learning model to produce Europe-wide PM_{2.5} forecasts at 1 km spatial resolution. Evaluated on 2,971 EEA stations across 362 days, CRAN-PM achieves RMSE = 6.85 $\mu\text{g}/\text{m}^3$ at T+1, outperforming all baselines by 4.7–10.7% and reducing bias at complex-terrain stations by 36%.

2 Related Work

Vision Transformers for high-resolution and multi-scale prediction. ViT [10] demonstrated that pure self-attention over image patches matches convolutional networks at scale, but its $\mathcal{O}(n^2)$ complexity limits large images. Swin Transformer [21] introduced shifted-window attention with linear complexity, enabling higher-resolution inputs but restricting receptive fields locally. PVT [33] and Twins [9] reduce quadratic cost via spatial-reduction attention while preserving multi-scale features. Video Swin [22] and TimeSformer [2] extend attention to spatio-temporal data but remain limited to moderate resolutions. CrossViT [5] exchanges information between two scales via class tokens, yet both branches operate on the same image domain. HIPT [8] and TransMIL [29] process patches independently without cross-scale interaction. CRAN-PM overcomes this via cross-resolution attention, allowing local high-resolution tokens to query a separately encoded global representation.

Data-driven weather and air quality prediction. AI weather models such as Pangu-Weather [3], GraphCast [17], FourCastNet [25], ClimaX [24], and Aurora [4] achieve strong forecasting skill at 0.1–0.25° resolution. FuXi [7] and GenCast [27] extend horizons but remain $\geq 0.25^\circ$. Satellite products such as GHAP [34] provide retrospective 1 km PM_{2.5} estimates, and CAMS [13] operates near 0.4°. Station-based models using gradient-boosted trees [6] or GNNs [32] lack spatial continuity. CRAN-PM bridges the gap by enabling 1 km continental prediction through explicit cross-resolution attention.

Physics-guided deep learning. Physical knowledge has been incorporated via PDE-constrained losses [23, 26, 28], latent physics-residual decompositions [18], hybrid advection-generation models [37], and Fourier Neural Operators [19, 20]. Building on single-scale physics-guided models TopoFlow [16] and AQ-Net [15], we encode physics as architectural inductive biases: elevation-aware attention and wind-guided cross-attention inject topographic and advective structure directly within attention.

3 Method

3.1 Cross-Resolution Attention for Ultra-High-Resolution ViTs

Forecasting PM_{2.5} at European scale and 1 km resolution requires processing ~ 29 million pixels per map. Tokenizing with 16×16 patches yields $\sim 115,000$ tokens, making naive self-attention intractable. Windowed attention (e.g., Swin [21]) is feasible but confines tokens locally, discarding the large-scale meteorological context essential for day-to-day pollution dynamics.

We adopt a divide-and-conquer strategy: coarse meteorological data (25 km) and fine PM_{2.5} (1 km) are split into global tokens and local tiles. Our **cross-resolution attention** lets local tokens query global tokens for large-scale context, preserving long-range dependencies while reducing memory to under 2 GB per tile. Inference over the full 29-million-pixel pan-European map completes in 1.8 seconds on a single GPU.

Fig. 2 shows CRAN-PM’s overall architecture: (1) the **global branch** takes coarse meteorological data across Europe (25 km, 168×280 patches, 735 tokens); (2) the **local branch** processes current-day fine-resolution PM_{2.5} (1 km) into 126 overlapping 512×512 tiles; (3) the **cross-attention module** learns long-range correlations between

local $PM_{2.5}$ and global meteorology; (4) upsampling blocks reconstruct the residual, added to today’s $PM_{2.5}$ observation.

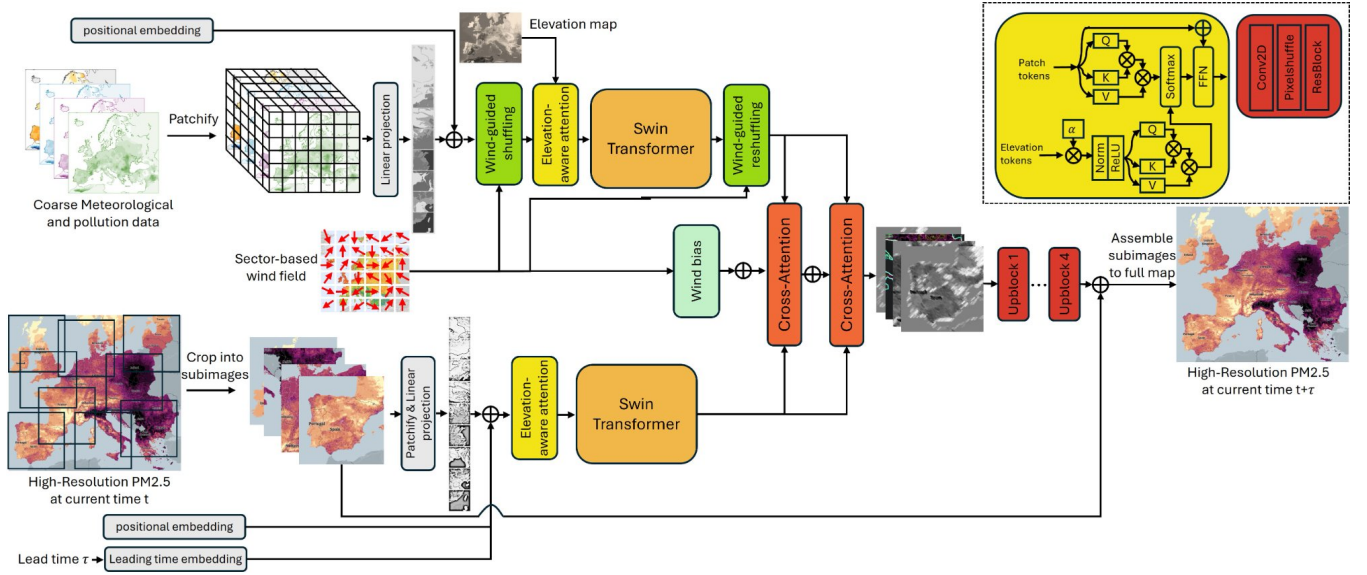


Figure 2: Architecture of CRAN-PM. A global branch (top) encodes coarse meteorological fields with wind-guided token reordering and elevation-aware attention; a local branch (bottom) encodes high-resolution $PM_{2.5}$ subimages. Two wind-biased cross-attention layers fuse the branches (fine queries coarse). A PixelShuffle-based Upblock (red inset) reconstructs the residual. The yellow inset details elevation-aware attention.

3.2 Problem Formulation

Let $\mathbf{x}_t^g \in \mathbb{R}^{70 \times 168 \times 280}$ denote the coarse input at day t , comprising ERA5 reanalysis (60 channels at days t and $t-1$) concatenated with CAMS composition forecasts (10 channels) at 0.25° . The fine input $\mathbf{x}_t^l \in \mathbb{R}^{5 \times 512 \times 512}$ is a local tile of fine-resolution $PM_{2.5}$ at days t and $t-1$, plus elevation, latitude, and longitude at 0.01° . For lead time $\tau \in \{1, 2, 3\}$ days:

$$\hat{y}_{t+\tau} = x_t^l + f_\theta(\mathbf{x}_t^g, \mathbf{x}_t^l, \tau), \quad (1)$$

where f_θ outputs a residual map Δ modelling daily changes. This delta formulation initialises the network near persistence, simplifying learning [3, 17].

3.3 Multi-Scale Encoder

Global branch. The coarse input is partitioned into 8×8 patches yielding $N_g = 735$ tokens projected to $d_g = 768$. Sinusoidal 2D positional embeddings are added, followed by one elevation-aware attention block (Sec. 3.4) and one Swin Transformer.

Local branch. Each 512×512 tile is tokenized with 16×16 patches, producing $N_l = 1,024$ tokens at $d_l = 512$. A learnable lead-time embedding $\mathbf{E}_{\text{lead}}(\tau) \in \mathbb{R}^{512}$ is added, followed by one elevation-aware attention block ($E_0 = 500$ m) and one Swin Transformer.

Wind-guided shuffling. Before the global transformer, each 7×7 patch group is reordered according to the local wind field. The ERA5 mean wind vector is quantized into one of 16 directional sectors (22.5° each), and patches are scanned upwind to downwind, aligning sequential processing with the physical advection path [16].

3.4 Elevation-Aware Attention

For token pair (i, j) with mean elevations E_i and E_j :

$$B_{ij}^{\text{elev}} = -\alpha \cdot \text{ReLU}\left(\frac{E_j - E_i}{E_0}\right), \quad B_{ij}^{\text{elev}} \in [-10, 0], \quad (2)$$

where α is learnable and $E_0 = 1,000$ m (global) or 500 m (local). This asymmetric bias penalizes attention to higher-elevation sources, consistent with katabatic flows [35]:

$$\text{Attn}_{\text{elev}} = \text{softmax}\left(\frac{\mathbf{Q}\mathbf{K}^\top}{\sqrt{d_h}} + \mathbf{B}^{\text{elev}} + \mathbf{B}^{\text{rel}}\right)\mathbf{V}. \quad (3)$$

3.5 Wind-Guided Cross-Attention

Local tokens query global tokens for large-scale context. Global tokens are projected to match local dimension: $\tilde{\mathbf{Z}}^g = \text{Linear}(\mathbf{Z}^g) \in \mathbb{R}^{735 \times 512}$. A wind-guided bias encodes upwind alignment:

$$\gamma_{ij} = \frac{(\mathbf{p}_i - \mathbf{p}_j)}{\|\mathbf{p}_i - \mathbf{p}_j\|} \cdot \frac{(u_{10,i}, v_{10,i})}{\|(u_{10,i}, v_{10,i})\|}, \quad B_{ij}^{\text{wind}} = \beta \cdot \gamma_{ij}, \quad (4)$$

$$\text{CrossAttn} = \text{softmax}\left(\frac{\mathbf{Q}\mathbf{K}^\top}{\sqrt{d_h}} + \mathbf{B}^{\text{wind}}\right)\mathbf{V}, \quad (5)$$

where β is learnable per head. Two successive cross-attention layers with residual connections and FFNs progressively integrate coarse-scale context.

3.6 Decoder

Fused local tokens are reshaped to $512 \times 32 \times 32$. Four upsampling blocks (Conv + PixelShuffle [30] + residual) progressively restore 512×512 resolution. A final zero-initialized 1×1 convolution outputs residual Δ , added to x_t^ℓ .

3.7 Training Objective

$$\mathcal{L} = \mathcal{L}_{\text{pixel}} + \lambda_{\text{FFL}} \mathcal{L}_{\text{FFL}} + \lambda_{\text{station}} \mathcal{L}_{\text{station}}, \quad (6)$$

where $\mathcal{L}_{\text{pixel}}$ is MSE over land pixels, \mathcal{L}_{FFL} is the focal frequency loss [14] emphasizing high-frequency errors, and $\mathcal{L}_{\text{station}}$ anchors predictions to $N_s = 2,971$ EEA stations. We set $\lambda_{\text{FFL}} = \lambda_{\text{station}} = 0.1$.

4 Experiments

4.1 Data

Our domain covers Europe (33°N – 72°N , 25°W – 45°E) at 1 km resolution ($4,192 \times 6,992$ pixels, 126 overlapping 512×512 tiles). Coarse inputs ($C_g = 70$ channels, ~ 25 km) combine **ERA5 reanalysis** (60 channels at days t and $t-1$) and **CAMS analysis** [13] (10 channels at days t and $t-1$). Fine inputs ($C_\ell = 5$ channels, ~ 1 km) comprise

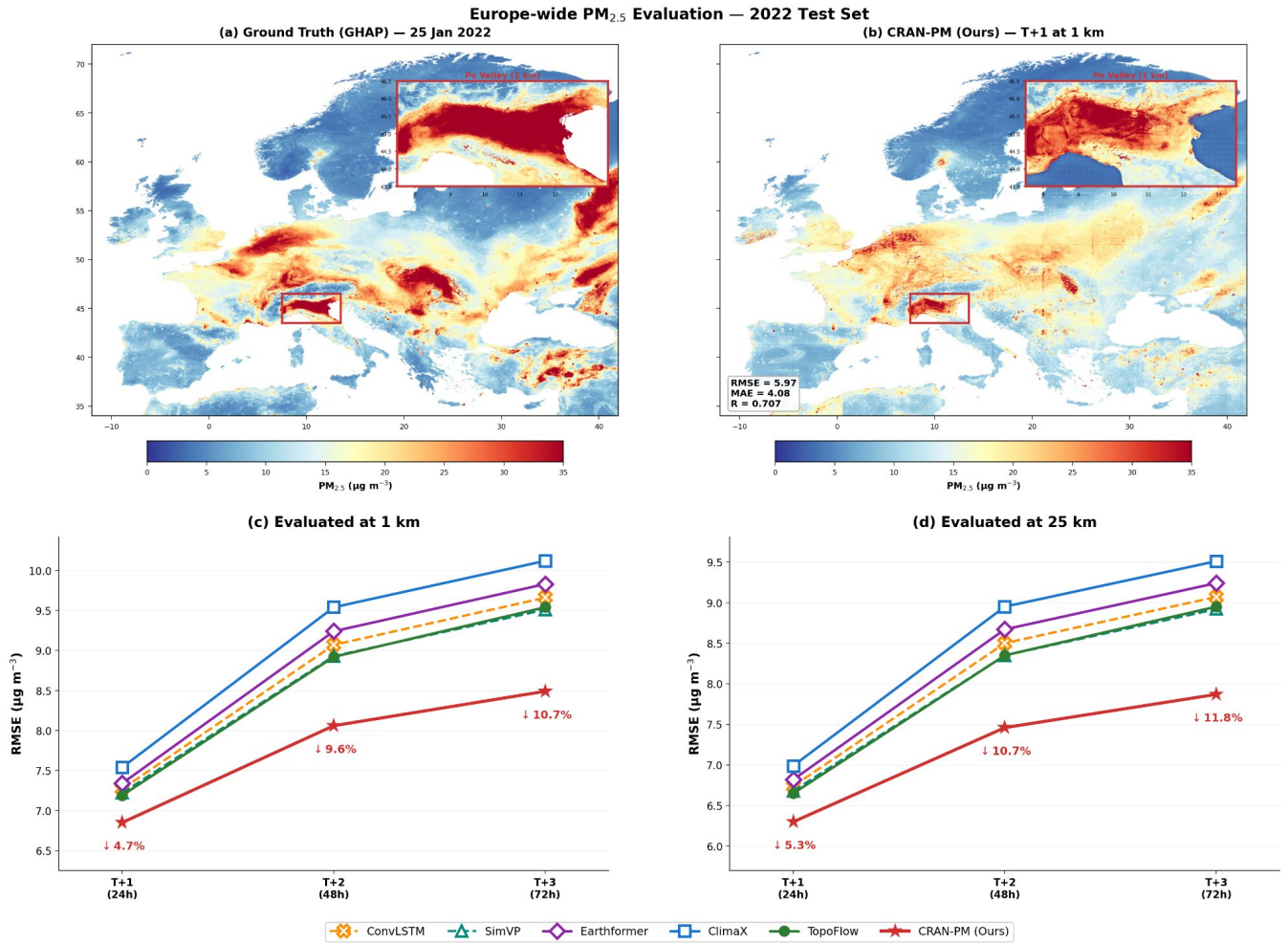


Figure 3: Europe-wide $PM_{2.5}$ evaluation (2022). (a) GT (GHAP, 1 km), Jan. 25, 2022. (b) CRAN-PM T+1; inset: Po Valley. (c,d) RMSE across T+1–T+3 at 1 km and 25 km. CRAN-PM (red stars) consistently outperforms all baselines.

GHAP [34] satellite-derived $PM_{2.5}$ at t and $t-1$, plus SRTM elevation, latitude, longitude. We train on 2017–2021 and test on 2022 (362 days, strictly temporal split, zero leakage).

4.2 Implementation Details

Global branch: $d_g = 768$, 8 blocks (1 elevation-aware + 7 Swin), 12 heads, patch 8×8 . Local branch: $d_\ell = 512$, 6 blocks (1 + 5), 8 heads, patch 16×16 . Cross-attention bridge: 2 layers, 8 heads, head dim 64. Total: 96 M parameters. Training: 64 AMD MI250X GPUs (LUMI supercomputer), 30 epochs, AdamW ($\text{lr} = 5 \times 10^{-5}$), cosine schedule, bfloat16 mixed precision, ≈ 860 GPU-hours. Inference: 1.8 s/map on one MI250X GPU.

4.3 Baselines

We compare against CAMS[†] [13], ConvLSTM [31], SimVP [11], Earthformer [12], ClimaX [24], and TopoFlow [16]. All learned baselines operate at 25 km and are bilinearly interpolated to 1 km for high-resolution evaluation; for 25 km evaluation, CRAN-PM is spatially averaged.

4.4 Main Results

Table 1: Quantitative comparison on European PM_{2.5} prediction. *Top:* evaluated at 1 km (coarser methods bilinearly interpolated). *Bottom:* evaluated at 25 km (CRAN-PM spatially averaged). †: zero-shot. **Bold:** best. Underline: second best.

Method	Res.	#Param	T+1 (24 h)				T+2 (48 h)				T+3 (72 h)			
			RMSE↓	MAE↓	SSIM↑	Δ(%)	RMSE↓	MAE↓	SSIM↑	Δ(%)	RMSE↓	MAE↓	SSIM↑	Δ(%)
<i>Evaluated at 1 km resolution</i>														
CAMS† [13]	1 km	–	12.35	7.34	0.38	–	12.41	7.45	0.36	–	12.45	7.51	0.34	–
ConvLSTM [31]	25 km	8.2M	7.27	3.24	0.48	–	9.07	4.08	0.45	–	9.66	4.44	0.42	–
SimVP [11]	25 km	4.9M	7.22	3.27	0.51	–	8.93	4.05	0.48	–	<u>9.51</u>	<u>4.40</u>	0.45	–
Earthformer [12]	25 km	61M	7.34	3.31	0.49	–	9.24	4.14	0.46	–	9.83	4.50	0.44	–
ClimaX [24]	25 km	57M	7.54	3.22	0.47	–	9.54	4.15	0.44	–	10.12	4.52	0.41	–
TopoFlow [16]	25 km	61M	<u>7.19</u>	<u>3.31</u>	<u>0.53</u>	–	<u>8.92</u>	<u>4.10</u>	<u>0.50</u>	–	9.54	4.47	<u>0.47</u>	–
CRAN-PM (ours)	1 km	96M	6.85	3.14	0.78	↓4.7	8.06	3.79	0.74	↓9.6	8.49	4.07	0.71	↓10.7
<i>Evaluated at 25 km resolution</i>														
CAMS† [13]	25 km	–	11.96	7.13	0.58	–	12.02	7.23	0.55	–	12.05	7.28	0.53	–
ConvLSTM [31]	25 km	8.2M	6.74	2.80	0.74	–	8.50	3.60	0.70	–	9.07	3.95	0.67	–
SimVP [11]	25 km	4.9M	6.68	2.83	0.77	–	8.35	3.57	0.73	–	<u>8.92</u>	<u>3.90</u>	0.69	–
Earthformer [12]	25 km	61M	6.82	2.91	0.75	–	8.67	3.69	0.71	–	9.24	4.03	0.68	–
ClimaX [24]	25 km	57M	6.99	2.72	0.73	–	8.95	3.62	0.69	–	9.51	3.97	0.65	–
TopoFlow [16]	25 km	61M	<u>6.65</u>	<u>2.85</u>	<u>0.79</u>	–	<u>8.35</u>	<u>3.61</u>	<u>0.75</u>	–	8.95	3.97	<u>0.72</u>	–
CRAN-PM (ours)	1 km	96M	6.30	2.85	0.84	↓5.3	7.46	3.46	0.80	↓10.7	7.87	3.72	0.76	↓11.8

Table 1 shows that at 1 km, CRAN-PM achieves RMSE=6.85 at T+1 (−4.7% vs. TopoFlow 7.19). The improvement widens at longer horizons: −9.6% at T+2 and −10.7% at T+3. SSIM of 0.78 vs. 0.53 reflects fine-scale spatial structure that interpolated 25 km models cannot capture. At 25 km, CRAN-PM remains the best method (−5.3% RMSE at T+1), confirming improvements stem from better predictions rather than resolution alone.

Table 2 reports validation against EEA ground stations.

Table 2: Validation against EEA ground monitoring stations (2022, T+1). Stations grouped by terrain complexity (σ_z : elevation s.d. within 25 km radius). **Bold:** best. †: physical model.

Method	All Stations ($N=2971$)				Flat ($\sigma_z < 50$ m, $N=2096$)				Complex ($\sigma_z \geq 50$ m, $N=875$)			
	RMSE↓	MAE↓	SSIM↑	Bias	RMSE↓	MAE↓	SSIM↑	Bias	RMSE↓	MAE↓	SSIM↑	Bias
CAMS†	13.08	6.16	0.52	−3.48	10.83	6.26	0.58	−3.81	17.35	5.90	0.45	−2.69
ConvLSTM [31]	11.94	4.96	0.68	−1.14	9.18	4.96	0.72	−1.04	16.80	4.95	0.58	−1.39
SimVP [11]	11.91	4.97	0.70	−1.14	9.14	4.97	0.73	−1.05	16.79	4.97	0.60	−1.37
Earthformer [12]	11.91	5.02	0.69	−1.18	9.16	5.03	0.72	−1.12	16.75	5.00	0.59	−1.32
ClimaX [24]	11.97	5.02	0.67	−1.13	9.22	5.01	0.71	−1.00	16.79	5.04	0.57	−1.44
TopoFlow [16]	12.01	4.96	0.71	−1.49	9.21	4.95	0.74	−1.38	16.91	4.98	0.62	−1.77
CRAN-PM (ours)	11.75	4.84	0.78	−0.86	8.94	4.86	0.80	−0.75	16.67	4.78	0.75	−1.13

CRAN-PM achieves the best metrics across all station categories. The improvement is most pronounced for complex terrain ($\sigma_z \geq 50$ m): bias reduced from −1.77 (TopoFlow) to −1.13, a 36% reduction, demonstrating the effectiveness of elevation-aware attention.

Figure 4 reveals that CRAN-PM closely tracks the observed PM_{2.5} seasonal cycle across all six European regions

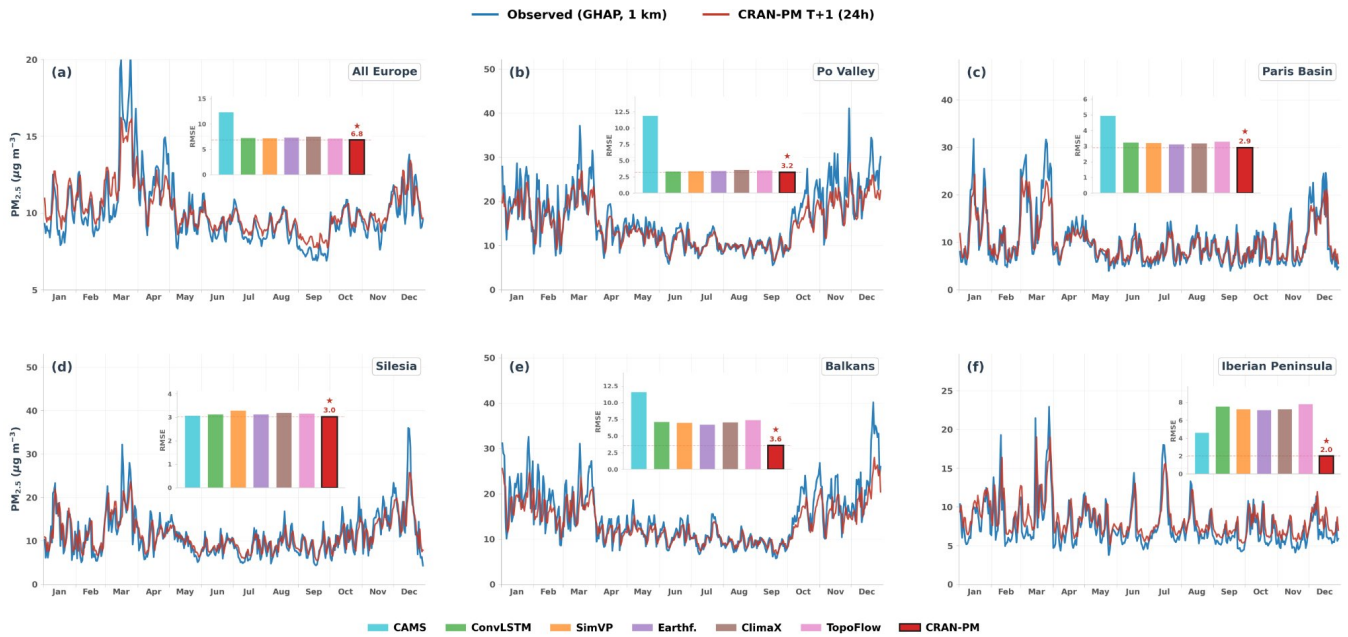


Figure 4: Temporal $PM_{2.5}$ evolution (2022, T+1). Blue: GHAP; red: CRAN-PM. Six regions. CRAN-PM achieves lowest RMSE in all regions.

throughout the 2022 test year. Winter peaks driven by residential heating and temperature inversions are accurately reproduced, as are summer minima associated with increased boundary layer height and enhanced precipitation scavenging. The inset RMSE bar plots confirm that CRAN-PM achieves the lowest error in every region, with the largest absolute improvements in high-pollution areas such as the Po Valley and Silesia, where complex orographic confinement amplifies $PM_{2.5}$ accumulation events.

CRAN-PM accurately captures episodic events, including spring biomass burning plumes in the Balkans and persistent winter smog events in central Europe. The wind-guided patch reordering and elevation-aware attention are particularly beneficial for these events: by aligning token sequences with the local advection field, the model anticipates the spatial direction of plume transport rather than relying solely on persistence. Degradation from T+1 to T+3 (Table 1) indicates that the learned atmospheric dynamics remain physically consistent over the 72-hour forecast horizon, without spurious error accumulation across lead times.

Regional variability in RMSE reflects underlying differences in emission density and meteorological complexity. The Iberian Peninsula records the lowest CRAN-PM RMSE among all six regions ($2.0 \mu\text{g m}^{-3}$, Fig. 4f), consistent with its predominantly marine boundary layer, low industrial emission density, and frequent Atlantic ventilation that suppresses $PM_{2.5}$ accumulation. Paris Basin follows closely at $2.9 \mu\text{g m}^{-3}$ (panel c). The Balkans present the highest regional error at $3.6 \mu\text{g m}^{-3}$ (panel e), driven by episodic wildfire plumes from outside the training region and steep orographic gradients between the Dinaric Alps and the Adriatic coast. Po Valley ($3.2 \mu\text{g m}^{-3}$) and Silesia ($3.0 \mu\text{g m}^{-3}$) also show elevated errors attributable to intense industrial sources and thermally stable basin geometries that concentrate $PM_{2.5}$ at sub-kilometre scales not fully resolved by ERA5 boundary layer parameterisations. These fine-scale emission hotspots represent the primary source of irreducible uncertainty in the current architecture.

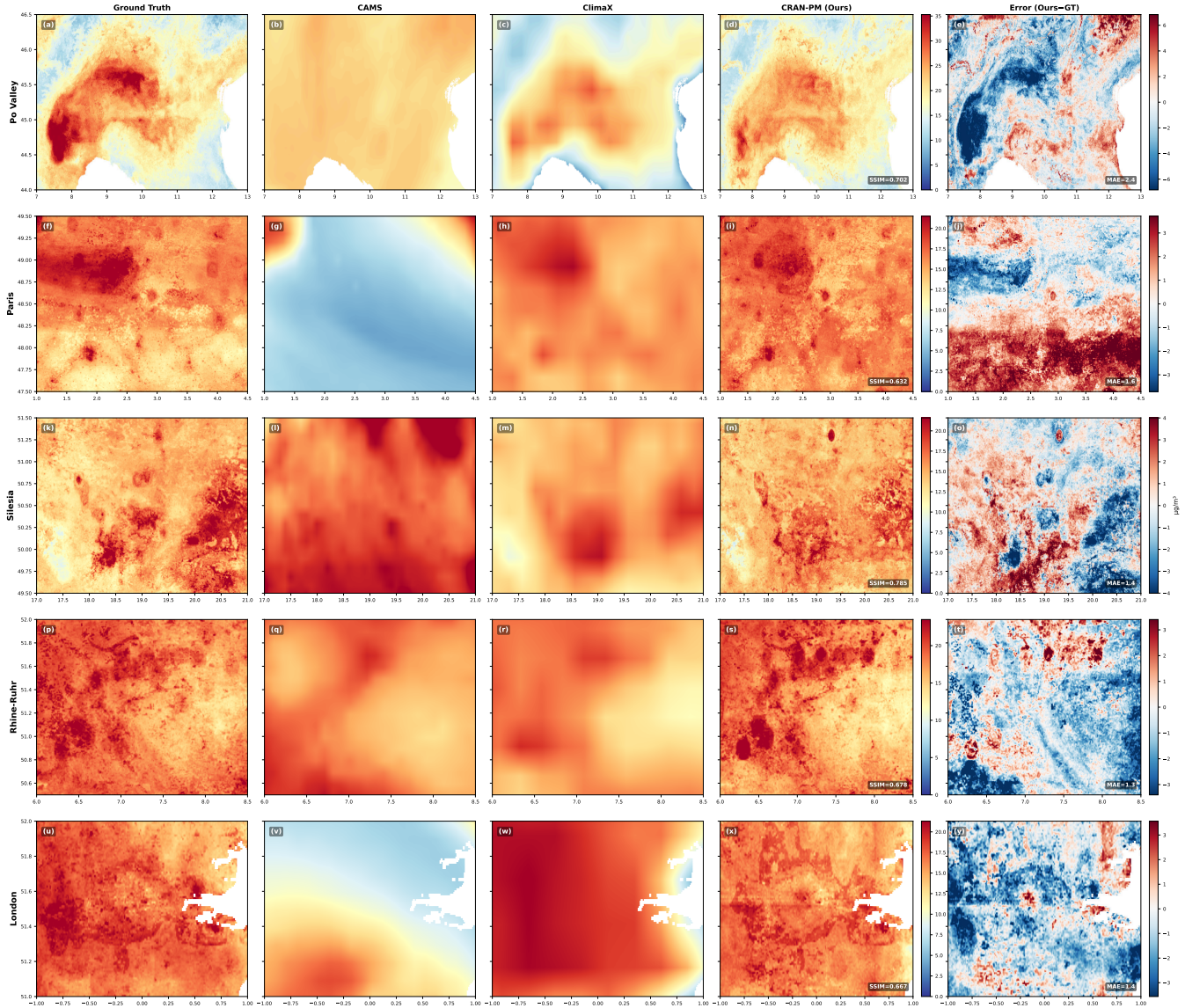


Figure 5: Regional $PM_{2.5}$ comparison at 1 km (T+1). Rows: Po Valley, Paris, Silesia, Rhine-Ruhr, London. (a) GT, (b) CAMS, (c) ClimaX, (d) CRAN-PM, (e) error (SSIM \geq 0.63).

4.5 Ablation Study

(a) Cross-attention fusion. Cross-resolution attention (row vii, 4.952) outperforms all alternatives. Removing cross-attention (row i, +0.150) is the largest single degradation. The reverse direction (row v, +0.082) validates the physical asymmetry: local $PM_{2.5}$ responds to large-scale meteorology, not vice versa.

(b) Progressive improvements. Larger effective batch (-0.14) stabilises training across heterogeneous tiles. Focal frequency loss (-0.06) sharpens gradients at urban-rural boundaries. Station loss and day-1 context (-0.09) correct satellite retrieval biases and provide atmospheric tendency.

(c) Removal study. Cross-scale attention (+0.43) and delta prediction (+0.23) are the two most critical components. Physics-guided biases jointly contribute +0.31 (R2+R3).

Table 3: Ablation study. (a) Cross-attention fusion strategy. (b) Progressive improvements. (c) Removal study. Val RMSE ($\mu\text{g}/\text{m}^3$) at T+1, 2022 European test set.

		Coarse Branch	Cross-Scale Attn	Elev. Bias	Wind Scan/Bias	PixelShuffle Dec.	Delta Prediction	FFL ($\lambda=0.1$)	Station Loss ($\lambda=0.1$)	Day-1 Context	Val RMSE \downarrow	Δ	
<i>(a) Cross-attention fusion design</i>													
		Q	K/V	<i>all other components fixed</i>									
(i)	No cross-attention	-	-								5.102	+0.150	
(ii)	Feature addition	Sum									5.021	+0.069	
(iii)	FiLM conditioning	Modul.									5.036	+0.084	
(iv)	Concat + Self-Attn	Joint									5.040	+0.088	
(v)	Coarse queries Fine	Coarse	Fine								5.034	+0.082	
(vi)	Bidirectional	Both	Both								5.015	+0.063	
(vii)	Cross-resolution attention (ours)	Fine	Coarse								4.952	ref.	
<i>(b) Progressive improvements</i>													
(A)	Baseline (MSE only)	Fine	Coarse	✓	✓	✓	✓	✓	✗	✗	✗	5.24	ref.
(B)	+ Eff. batch size	Fine	Coarse	✓	✓	✓	✓	✓	✗	✗	✗	5.10	-0.14
(C)	+ Focal Frequency Loss	Fine	Coarse	✓	✓	✓	✓	✓	✓	✗	✗	5.04	-0.06
(D)	+ Station loss & day-1	Fine	Coarse	✓	✓	✓	✓	✓	✓	✓	✓	4.95	-0.09
<i>(c) Removal study (from full CRAN-PM)</i>													
CRAN-PM (full)		Fine	Coarse	✓	✓	✓	✓	✓	✓	✓	✓	4.95	ref.
(R1)	- Cross-scale attention	-	-	✓	✗	✓	✓	✓	✓	✓	✓	5.38	+0.43
(R2)	- Elevation bias	Fine	Coarse	✓	✓	✗	✓	✓	✓	✓	✓	5.12	+0.17
(R3)	- Wind scan & bias	Fine	Coarse	✓	✓	✓	✗	✓	✓	✓	✓	5.09	+0.14
(R4)	- PixelShuffle (ConvT)	Fine	Coarse	✓	✓	✓	✓	✗	✓	✓	✓	5.08	+0.13
(R5)	- Delta prediction	Fine	Coarse	✓	✓	✓	✓	✓	✗	✓	✓	5.18	+0.23
(R6)	- FFL	Fine	Coarse	✓	✓	✓	✓	✓	✓	✗	✓	5.07	+0.12
(R7)	- Station loss	Fine	Coarse	✓	✓	✓	✓	✓	✓	✓	✗	5.02	+0.07
(R8)	- Day-1 context	Fine	Coarse	✓	✓	✓	✓	✓	✓	✓	✗	5.04	+0.09

Table 3 shows a clear ranking of components: the cross-resolution attention bridge provides the single largest performance gain, confirming that fusing coarse meteorological context with fine observations is the core architectural innovation. The elevation bias (R2, +0.17) and wind scan (R3, +0.14) contribute comparably, reflecting the physical importance of orographic confinement and advection for $PM_{2.5}$ accumulation over complex terrain. Delta prediction (R5, +0.23) is the second most critical component, as initialising the network output to today’s $PM_{2.5}$ field reduces the learning burden: the model only needs to predict the daily change rather than the absolute concentration, which eases optimisation for a residual mapping near zero over clean-air days.

The progressive improvement experiment (Table 3b) demonstrates that each training innovation is independently beneficial and their combination is approximately additive. The focal frequency loss targets a well-known weakness of ℓ_2 -based objectives: the tendency to over-smooth sharp spatial gradients at emission source boundaries. Station loss ($\lambda_{\text{station}} = 0.1$) anchors predictions to ground-measured concentrations, reducing the systematic negative bias inherited from GHAP satellite retrievals in complex terrain. The day-1 context input adds an atmospheric tendency that helps the model capture short-term trends without explicit recurrence.

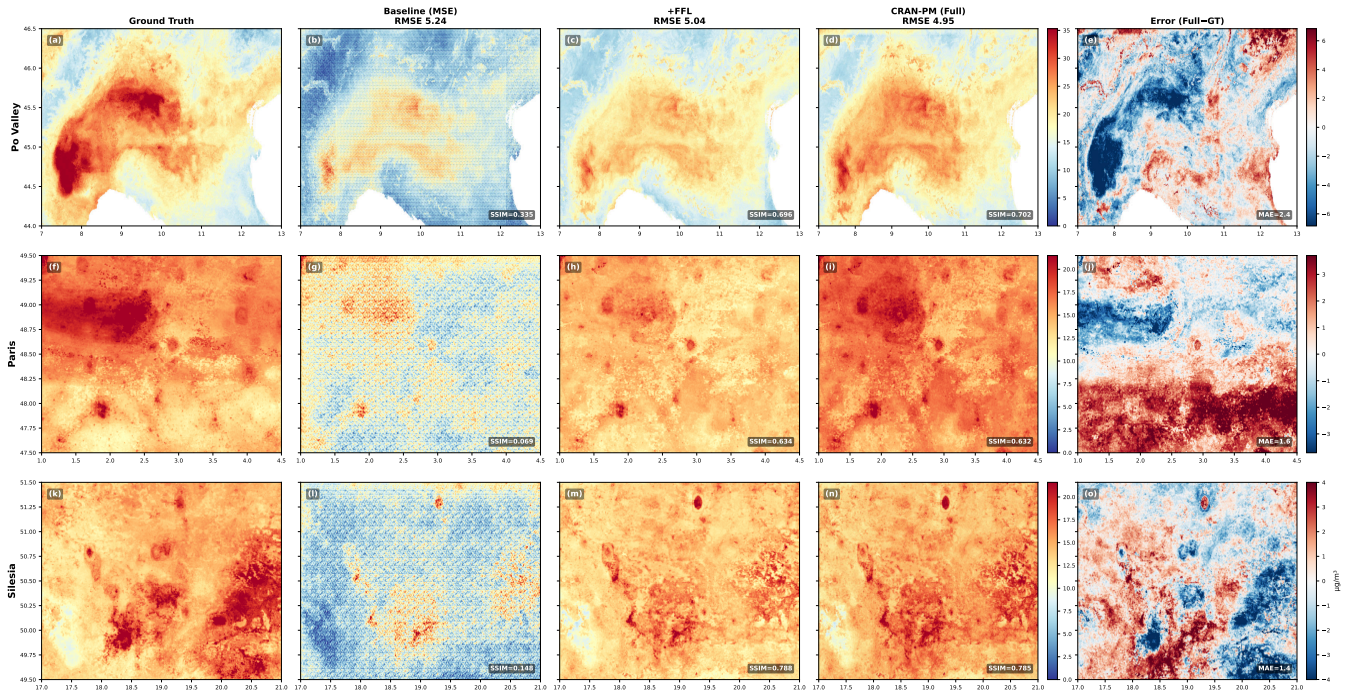


Figure 6: Ablation: progressive improvements at 1 km (T+1). (a) GT, (b) baseline (SSIM ≤ 0.34), (c) +FFL, (d) CRAN-PM full (RMSE = 4.95), (e) error.

Limitations and Discussion While CRAN-PM achieves strong results, several directions remain open. The model relies on GHAP satellite-derived PM_{2.5} as supervision, which carries retrieval uncertainties under clouds and complex terrain. The current temporal resolution is daily, whereas operational air quality management often benefits from hourly forecasts. The prediction horizon is limited to 1~3 days; extending it would require modelling non-stationary emissions and atmospheric chemistry. Finally, the fixed 512×512 tiling strategy could be improved with adaptive spatial partitioning.

5 Conclusion

We introduced **CRAN-PM**, a dual-branch Vision Transformer for ultra-high-resolution PM_{2.5} prediction. The key contribution is cross-resolution attention, linking global coarse-resolution meteorology with local high-resolution PM_{2.5} observation. The global branch captures large-scale context, while local branches model fine-scale details, and the cross-attention enables efficient information exchange across scales. This design preserves long-range dependencies while reducing peak memory from hundreds of gigabytes to under 2 GB per tile, with computation scaling linearly with domain size. Physics-guided attention biases, elevation-aware self-attention and wind-guided cross-attention, inject domain knowledge as soft priors for physical regularization, allowing the network to produce physically consistent prediction. On daily PM_{2.5} forecasting across Europe (2022), CRAN-PM achieves RMSE of $6.85 \mu\text{g}/\text{m}^3$ at 1 km (T+1), improving $4.7\sim 10.7\%$ over the strongest single-scale baseline and reducing bias at complex-terrain stations by 36%. More generally, cross-resolution attention offers a scalable mechanism for Vision Transformers in ultra-high-resolution tasks requiring global context, with potential applications in urban-scale environmental modeling and analysis.

References

- [1] Anurag Arnab et al. “ViViT: A Video Vision Transformer”. In: *ICCV*. 2021, pp. 6816–6826.
- [2] Gedas Bertasius, Heng Wang, and Lorenzo Torresani. “Is Space-Time Attention All You Need for Video Understanding?” In: *ICML*. 2021.
- [3] Kaifeng Bi et al. “Accurate medium-range global weather forecasting with 3D neural networks”. In: *Nature* 619 (2023), pp. 533–538.
- [4] Cristian Bodnar, Wessel P Bruinsma, et al. “Aurora: A Foundation Model of the Atmosphere”. In: *Nature* (2024).
- [5] Chun-Fu Chen, Quanfu Fan, and Rameswar Panda. “CrossViT: Cross-Attention Multi-Scale Vision Transformer for Image Classification”. In: *ICCV*. 2021.
- [6] Gang Chen et al. “Extreme Gradient Boosting model to estimate $PM_{2.5}$ ”. In: *Atmospheric Environment* 202 (2019), pp. 180–189.
- [7] Lei Chen et al. “FuXi”. In: *npj Climate and Atmospheric Science* (2023).
- [8] Richard J. Chen et al. “Scaling Vision Transformers to Gigapixel Images via Hierarchical Self-Supervised Learning”. In: *CVPR*. 2022.
- [9] Xiangxiang Chu et al. “Twins: Revisiting the Design of Spatial Attention in Vision Transformers”. In: *NeurIPS*. 2021.
- [10] Alexey Dosovitskiy, Lucas Beyer, Alexander Kolesnikov, et al. “An Image is Worth 16x16 Words: Transformers for Image Recognition at Scale”. In: *ICLR*. 2021.
- [11] Zhangyang Gao et al. “SimVP: Simpler yet Better Video Prediction”. In: *CVPR*. 2022.
- [12] Zhihan Gao, Xingjian Shi, Hao Wang, et al. “Earthformer”. In: *NeurIPS*. 2022.
- [13] Antje Inness, Melanie Ades, et al. “The CAMS reanalysis of atmospheric composition”. In: *Atmospheric Chemistry and Physics* 19.6 (2019), pp. 3515–3556.
- [14] Liming Jiang et al. “Focal Frequency Loss for Image Reconstruction and Synthesis”. In: *ICCV*. 2021, pp. 13919–13929.
- [15] Ammar Kheder et al. “Deep Spatio-Temporal Neural Network for Air Quality Reanalysis”. In: *Image Analysis: 23rd Scandinavian Conference, SCIA 2025*. Vol. 15725. Lecture Notes in Computer Science. Springer, 2025.
- [16] Ammar Kheder et al. “TopoFlow: Physics-guided Neural Networks for High-Resolution Air Quality Prediction”. In: *arXiv preprint arXiv:2602.16821* (2026).
- [17] Remi Lam, Alvaro Sanchez-Gonzalez, Matthew Willson, et al. “Learning skillful medium-range global weather forecasting”. In: *Science* 382.6677 (2023), pp. 1416–1421.
- [18] Vincent Le Guen and Nicolas Thome. “Disentangling Physical Dynamics from Unknown Factors”. In: *CVPR*. 2020, pp. 11474–11484.
- [19] Zongyi Li et al. “Fourier Neural Operator”. In: *ICLR* (2021).
- [20] Zongyi Li et al. “Physics-Informed Neural Operator”. In: *JMLR* (2024).
- [21] Ze Liu, Yutong Lin, Yue Cao, et al. “Swin Transformer: Hierarchical Vision Transformer Using Shifted Windows”. In: *ICCV*. 2021, pp. 10012–10022.
- [22] Ze Liu, Jia Ning, Yue Cao, et al. “Video Swin Transformer”. In: *CVPR*. 2022.
- [23] Zhi-Song Liu, Petri Clusius, and Michael Boy. “Neural network emulator for atmospheric chemical ODE”. In: *Neural Networks* 184 (2025), p. 107106.
- [24] Tung Nguyen et al. “ClimaX: A Foundation Model for Weather and Climate”. In: *ICML*. 2023.
- [25] Jaideep Pathak et al. “FourCastNet”. In: *arXiv preprint arXiv:2202.11214* (2022).
- [26] Wenqing Peng, Zhi-Song Liu, and Michael Boy. “SPIN-ODE”. In: *ECAI* (2025), pp. 2033–2040.
- [27] Ilan Price et al. “GenCast”. In: *Nature* (2024).
- [28] Maziar Raissi, Paris Perdikaris, and George E Karniadakis. “Physics-informed neural networks”. In: *Journal of Computational Physics* 378 (2019), pp. 686–707.
- [29] Zhuchen Shao et al. “TransMIL”. In: *NeurIPS*. 2021.
- [30] Wenzhe Shi, Jose Caballero, et al. “Real-Time Single Image and Video Super-Resolution Using an Efficient Sub-Pixel Convolutional Neural Network”. In: *CVPR*. 2016, pp. 1874–1883.

- [31] Xingjian Shi, Zhourong Chen, Hao Wang, et al. “Convolutional LSTM Network”. In: *NeurIPS*. 2015.
- [32] Shuo Wang et al. “PM_{2.5}-GNN”. In: *arXiv preprint arXiv:2002.12898* (2020).
- [33] Wenhai Wang et al. “Pyramid Vision Transformer”. In: *ICCV*. 2021.
- [34] Jing Wei, Zhanqing Li, Alexei Lyapustin, et al. “Reconstructing 1-km-resolution high-quality PM_{2.5} data records”. In: *Remote Sensing of Environment* 252 (2021), p. 112136.
- [35] C David Whiteman. *Mountain Meteorology: Fundamentals and Applications*. Oxford University Press, 2000.
- [36] Xi Ye and Guillaume-Alexandre Bilodeau. “VPTR: Efficient Transformers for Video Prediction”. In: *ICPR*. IEEE. 2022, pp. 3492–3499.
- [37] Yuchen Zhang, Mingsheng Long, et al. “Skilful nowcasting of extreme precipitation with NowcastNet”. In: *Nature* 619 (2023), pp. 526–532.

Supplementary Material

Cross-Resolution Attention Network for High-Resolution $PM_{2.5}$ Prediction

This supplementary material provides: (1) a scalability analysis motivating the dual-branch design, (2) zero-shot geographic transferability results on two out-of-distribution regions, and (3) complete architecture specifications, hyperparameters, test set stratification, input channels, and the forward pass algorithm.

S1 Architecture Overview and Scalability Motivation

At 1 km resolution, the full European domain yields **115 K tokens** requiring \sim **300 GB VRAM**, intractable due to $\mathcal{O}(N^2)$ attention. CRAN-PM solves this via scale decoupling (Fig. S1): a **Global Branch** encodes ERA5/CAMS (70 ch, 25 km) into Z_{global} once per day, while a **Local Branch** processes each 512×512 GHAP tile independently, fused by **Cross-Resolution Attention** (Q : local, KV : global, wind bias B^{wind}), yielding <2 GB/tile at \sim **1.8 s** per inference.

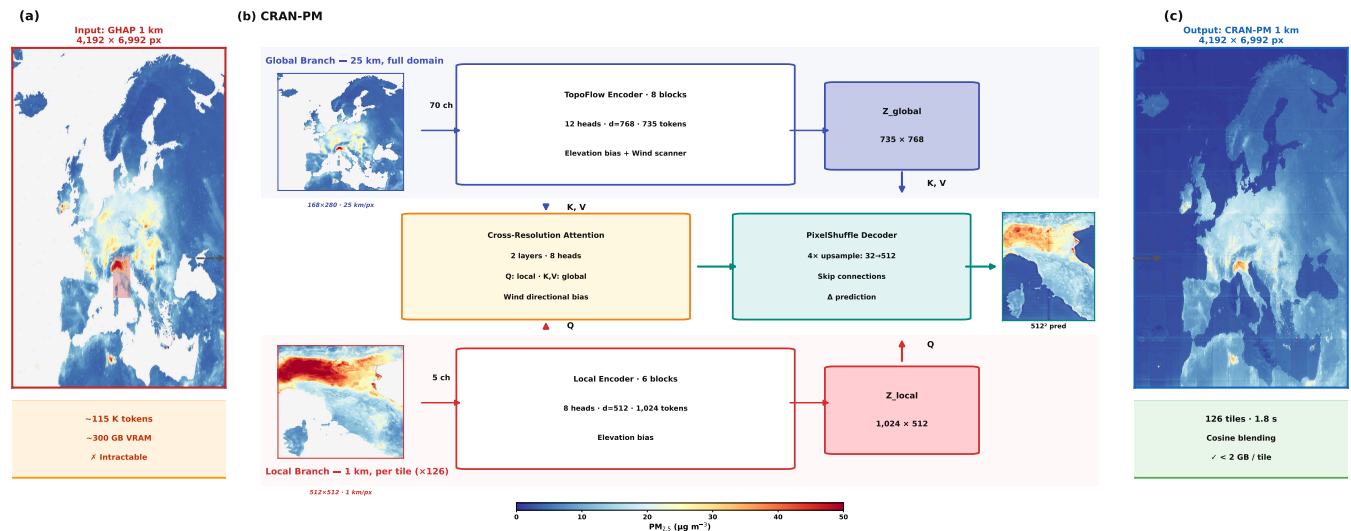


Figure S1: CRAN-PM architecture overview. *Left:* naive 1 km processing is intractable (\sim 115 K tokens, \sim 300 GB VRAM). *Centre:* dual-branch design with Global Branch (735 tokens, 25 km) and Local Branch (1,024 tokens/tile, 1 km), fused by Cross-Resolution Attention with wind bias. *Right:* full-domain output from 126 overlapping tiles with cosine blending (<2 GB/tile, \sim 1.8 s).

The tile-based inference strategy mitigates potential boundary artefacts by overlapping adjacent tiles by 64 pixels and applying a cosine blending weight that smoothly down-weights predictions near tile edges, yielding a seamless full-domain output. The shared Global Branch with cached daily representations (735×735 -token attention computed once per day and reused across all 126 local tiles) reduces total inference time by approximately 60% compared to a non-cached architecture, enabling full-domain $PM_{2.5}$ forecasts in under 4 minutes on a single AMD MI250X GPU.

Memory scaling is a key advantage of the tile-based approach. At inference, peak GPU memory per tile is under 2 GB, enabling deployment on any GPU with at least 4 GB HBM. At training time, a per-GPU batch of 2 tiles at bfloat16 precision fits within the 64 GB HBM of each AMD MI250X GCD. The daily caching of the Global Branch further reduces training memory: only the Local Branch and Cross-Resolution Attention are backpropagated per tile,

while the Global Branch gradient is accumulated once per day over all 126 tiles sharing the same meteorological forcing.

S2 Out-of-Distribution Generalisation

To assess geographic transferability, we apply the Europe-trained checkpoint zero-shot to two out-of-distribution regions using the same ERA5/CAMS/GHAP pipeline, with no domain adaptation or fine-tuning.

North America shares similar pollution regimes with Europe: wildfire-driven $PM_{2.5}$, comparable concentration ranges ($0\text{--}20\ \mu\text{g}/\text{m}^3$), and analogous orographic patterns (Rocky Mountains vs. European Alps), placing test samples largely within the training distribution. **India**, by contrast, presents a fundamentally different regime: the Indo-Gangetic Plain (IGP) experiences extreme anthropogenic pollution (up to $80\ \mu\text{g}/\text{m}^3$, i.e. $3\text{--}5\times$ the European training range), with emission sources (brick kilns, crop burning, dense vehicle traffic) that have no European equivalent.

For each region we report spatial maps (Fig. S2–S3) and annual mean scatter plots (Fig. S4) aggregating 365 daily predictions over millions of pixels.

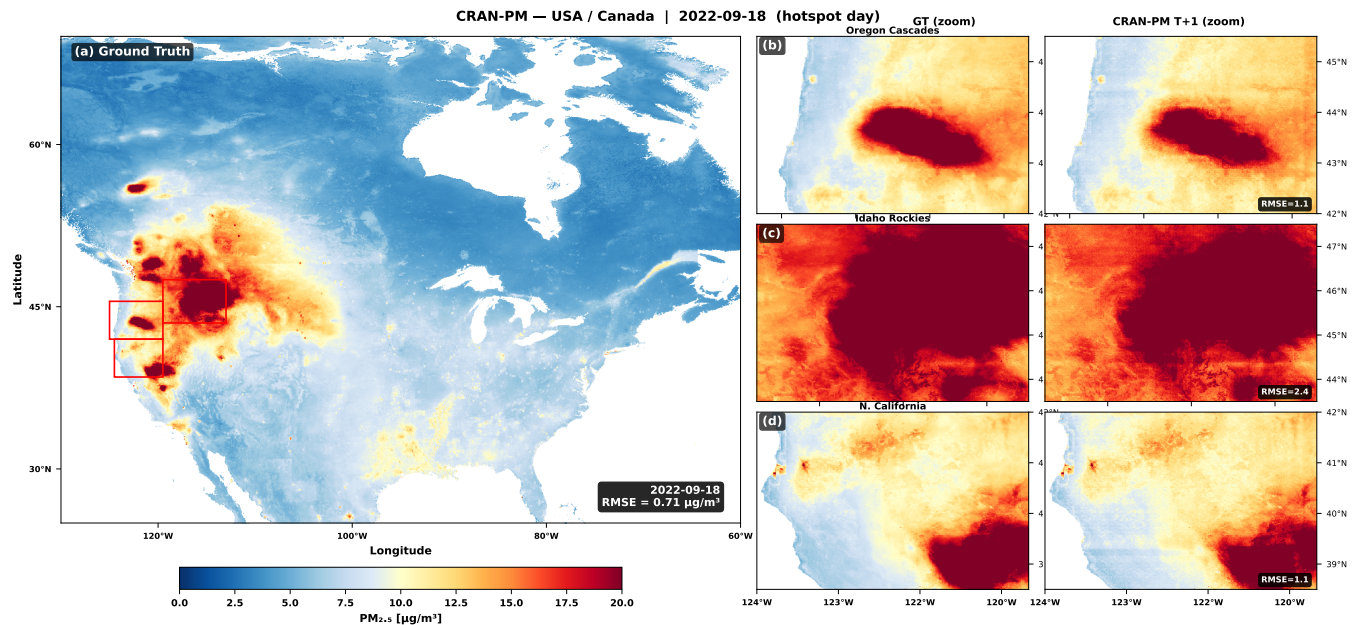


Figure S2: Zero-shot transfer to USA/Canada (2022-09-18, wildfire episode). RMSE = $0.71\ \mu\text{g}/\text{m}^3$ overall; Oregon Cascades = 1.1, Idaho Rockies = 2.4, N. California = 1.1.

The near-unity regression slope on USA/Canada ($y = 1.02x + 0.3$, $R^2 = 0.938$) suggests the model has internalised transferable representations of meteorology-driven $PM_{2.5}$ dynamics rather than memorising European spatial patterns. The India result confirms that transferability is bounded by the emission regime.

Practical implications. These zero-shot experiments suggest that CRAN-PM can be deployed with minimal adaptation in regions sharing European pollution meteorology, such as temperate North America or western Asia. For regions with structurally distinct emission regimes, such as the Indo-Gangetic Plain, a lightweight fine-tuning step on a small set of locally labelled GHAP tiles ($\sim 3\text{--}6$ months of data) is expected to close the performance gap, since the backbone meteorological representations learned from ERA5 remain broadly transferable across climatic zones. Future work will explore continual adaptation strategies that allow CRAN-PM to update its emission-regime priors without retraining the full model.

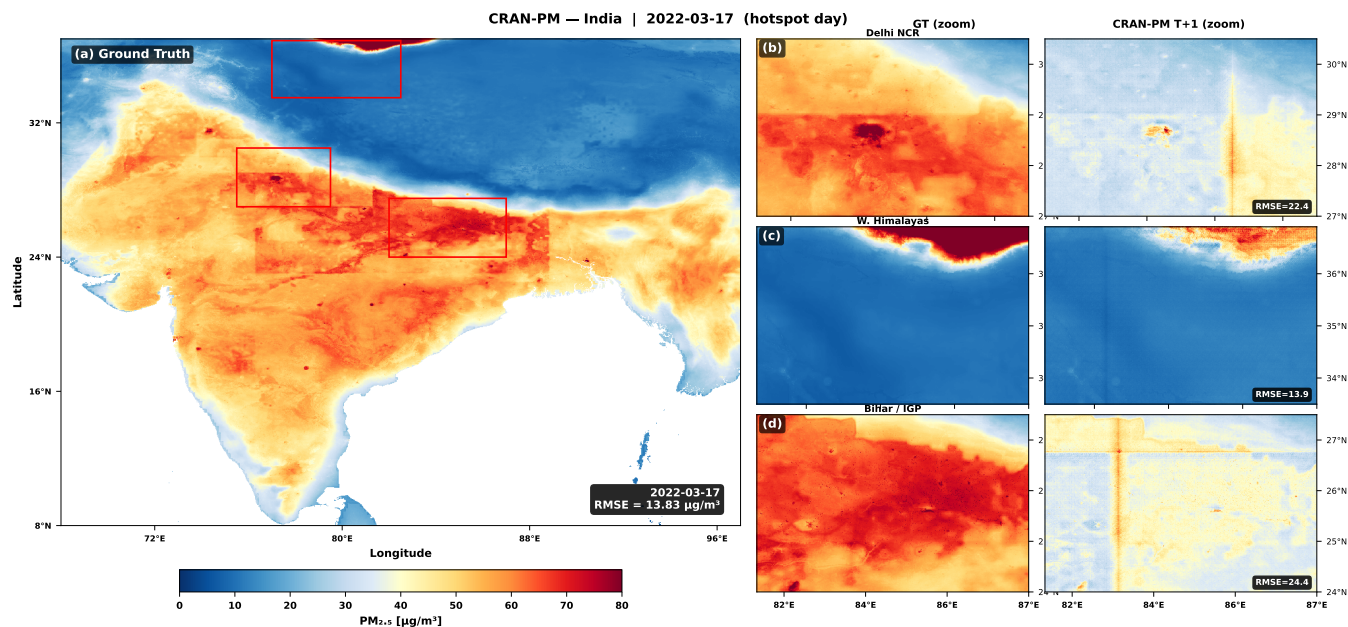


Figure S3: Zero-shot transfer to India (2022-03-17, IGP hotspot day). RMSE = $13.83 \mu\text{g}/\text{m}^3$ overall; Delhi NCR = 22.4, Bihar/IGP = 24.4. IGP concentrations (up to $80 \mu\text{g}/\text{m}^3$) are 3–5 \times the European training range.

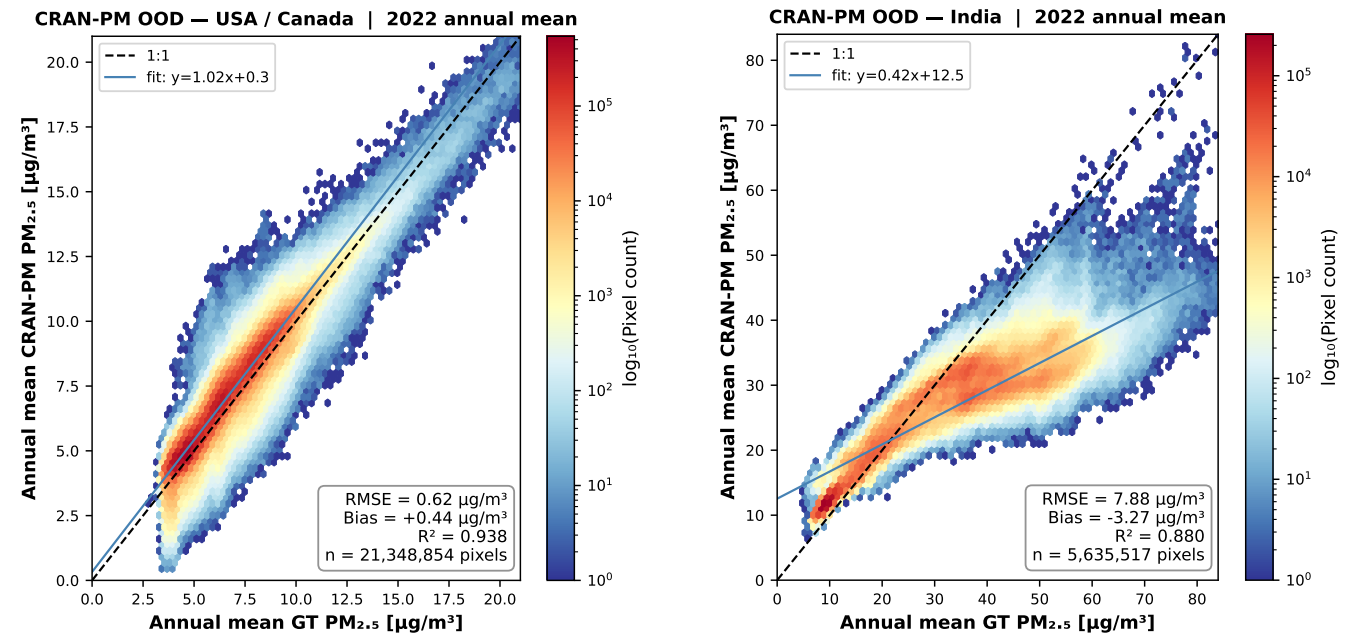


Figure S4: Annual mean scatter plots (2022) for both OOD regions. *Left* (USA/Canada): RMSE = 0.62, Bias = +0.44, $R^2 = 0.938$ ($n = 21.3\text{M}$ px); slope $y = 1.02x + 0.3$ confirms near-unity scaling. *Right* (India): RMSE = 7.88, Bias = -3.27, $R^2 = 0.880$ ($n = 5.6\text{M}$ px); systematic underestimation above $40 \mu\text{g}/\text{m}^3$.

S3 Architecture and Implementation Details

CRAN-PM is a 96 M-parameter dual-branch Vision Transformer. The **Global Branch** encodes ERA5/CAMS coarse inputs (70 channels, 25 km) into a 735-token representation \mathbf{Z}^g once per forecast day, cached across all 126 tiles. The **Local Branch** encodes each 512×512 GHAP tile (5 channels, 1 km) into 1024 tokens. A **Cross-Resolution**

Attention bridge fuses the two scales using wind-directional bias, and a **PixelShuffle decoder** reconstructs the full-resolution residual Δ , added back to today’s PM_{2.5} tile.

Table S1: Layer-by-layer architecture.

Table S1: CRAN-PM layer-by-layer architecture. 96 M parameters; FFN ratio 4.0; drop-path 0.1; input dropout 0.1.

Module	Input	Output	Config	Notes
<i>Global branch</i>				
Unfold + Linear	$70 \times 168 \times 280$	735×768	$k = s = 8$	rocBLAS
Sinusoidal 2D pos. embed	735×768	735×768	fixed	
Elevation-aware Attn	735×768	735×768	$h = 12, E_0 = 1000$ m	1 block
Swin Transformer	735×768	735×768	$h = 12$, win 7×7 , depth 7	shifted window
<i>Local branch (per tile)</i>				
Unfold + Linear	$5 \times 512 \times 512$	1024×512	$k = s = 16$	rocBLAS
Sinusoidal 2D pos. embed	1024×512	1024×512	fixed	
Lead-time embedding	$\tau \in \{1, 2, 3\}$	1024×512	learnable \mathbb{R}^{512}	broadcast
Elevation-aware Attn	1024×512	1024×512	$h = 8, E_0 = 500$ m	1 block
Swin Transformer	1024×512	1024×512	$h = 8$, win 8×8 , depth 5	
<i>Cross-resolution bridge</i>				
Linear projection	735×768	735×512	no bias	global \rightarrow local dim
Cross-Attn $\times 2$ + FFN	Q: 1024×512 , KV: 735×512	1024×512	$h = 8$, head dim 64	wind bias β per head
<i>PixelShuffle decoder</i>				
Reshape	1024×512	$512 \times 32 \times 32$		
Upblock $\times 4$ (Conv+PS+Res)		$32 \times 512 \times 512$	$r = 2$ each	
Conv 1×1 , zero-init	32×512	1×512		residual Δ

The Global Branch uses a larger Swin depth (7 blocks) than the Local Branch (5 blocks) to capture planetary-scale transport patterns. The elevation-aware attention block is placed before the Swin Transformer in each branch so that topographically-induced concentration gradients are encoded into the token representations before long-range spatial mixing. The PixelShuffle decoder operates at $r = 2$ per upsampling step (4 steps: $32 \rightarrow 64 \rightarrow 128 \rightarrow 256 \rightarrow 512$ pixels), which empirically outperformed a single-step transpose convolution at equivalent parameter count, likely because successive upsampling preserves high-frequency spatial structure more faithfully.

The test set is stratified to ensure balanced coverage across seasons, times of day, and days of the month (Table S2). Equal sample counts (1,000 per lead time) prevent any single temporal regime from dominating reported metrics. The balanced seasonal distribution is particularly important for PM_{2.5} evaluation: winter episodes (higher concentrations, stronger orographic gradients) and summer conditions (lower background, photochemical secondary formation) require qualitatively different predictive skills. All 4,000 test samples are drawn from 2022, providing a strictly out-of-sample evaluation with zero temporal leakage from the 2017–2021 training period.

Table S2: Test set stratification (year 2022, 4,000 samples).

Temporal Horizon	Seasonal Distribution				Daily Distribution				Day of Month			Total
	Winter (Jan–Mar)	Spring (Apr–Jun)	Summer (Jul–Sep)	Autumn (Oct–Dec)	Night (00–06)	Morning (06–12)	Afternoon (12–18)	Evening (18–24)	Days 1–10	Days 11–20	Days 21–31	
12h	255	262	245	238	234	270	227	269	338	329	333	1,000
24h	246	225	268	261	266	227	250	257	332	327	341	1,000
48h	252	254	278	216	260	233	273	234	342	311	347	1,000
96h	255	257	239	249	272	232	254	242	344	331	325	1,000
Total	1,008	998	1,030	964	1,032	962	1,004	1,002	1,356	1,298	1,346	4,000

Table S3: Training hyperparameters and LUMI infrastructure. Best checkpoint: epoch 18, val RMSE = 4.95, test RMSE = 6.85 $\mu\text{g}/\text{m}^3$.

Hyperparameter	Value	Hyperparameter	Value
Optimizer	AdamW	Weight decay	0.05
Learning rate	5×10^{-5}	Min LR (cosine)	1×10^{-6}
Warmup	5 epochs	LR schedule	cosine annealing
Max epochs	30	Best epoch	18
Per-GPU batch	2	Effective batch	128
Gradient clip	1.0 (global norm)	Precision	bfloat16-mixed
λ_{pixel}	1.0	λ_{FFL}	0.1
λ_{station}	0.1	Drop-path	0.1
Hotspot ratio	0.5	MLP ratio	4.0
E_0 global	1000 m	E_0 local	500 m
Wind sectors	16	Patch size global	8×8
Patch size local	16×16	Tile overlap	64 px

LUMI supercomputer

Nodes	4	GPUs	64 AMD MI250X GCDs
Total HBM	4,096 GB	Interconnect	Slingshot-11
PyTorch	2.2 (ROCm 6.0.3)	Strategy	PyTorch Lightning DDP
Wall time	≈ 11 h	Total GPU-hours	≈ 860

The cosine annealing schedule with a minimum LR of 1×10^{-6} provides gradual decay that prevents the model from converging prematurely on the heterogeneous tile distribution. The hotspot ratio (0.5) controls the fraction of training tiles sampled from high-pollution regions (Po Valley, Silesia, Rhine-Ruhr), ensuring sufficient exposure to extreme concentration events. Drop-path regularisation (0.1) is applied to both branches to prevent over-reliance on individual tokens during co-training of the dual-branch architecture. The choice of AdamW with weight decay (0.05) rather than standard Adam reflects the large parameter space of the Swin Transformer blocks, where ℓ_2 regularisation is known to improve generalisation on spatially structured prediction tasks.

Table S4: Input channel specification (70 coarse + 5 local = 75 total).

Variable	Symbol	Source	Norm.	#ch
<i>ERA5 surface, days t and $t-1$</i>				
10-m wind	u_{10}, v_{10}	ERA5	z-score	2
2-m temperature	T_{2m}	ERA5	z-score	1
Surface pressure	p_s	ERA5	z-score	1
Precipitation	tp	ERA5	z-score	1
<i>ERA5 pressure levels (500, 700, 850, 925, 1000 hPa), days t and $t-1$</i>				
u, v, T, z, q ($\times 5$ levels)		ERA5	z-score	25
<i>CAMS analysis, days t and $t-1$</i>				
PM _{2.5} , PM ₁₀ , NO ₂ , O ₃ , CO		CAMS	z-score	5
<i>Total coarse: $(5 + 25 + 5) \times 2$</i>				70
<i>Local tile (per 512×512)</i>				
GHAP PM _{2.5} at t and $t-1$		GHAP	$(x-15)/20$	2
SRTM elevation	h	SRTM	raw m	1
Latitude, Longitude		computed	degrees	2
<i>Total local</i>				5

Algorithm S1 CRAN-PM forward pass (single tile). Global branch (lines 1–3) computed once per day and cached. Local branch and cross-resolution attention (lines 4–8) run per tile.

Require: $\mathbf{x}^g \in \mathbb{R}^{70 \times 168 \times 280}$, $\mathbf{x}^\ell \in \mathbb{R}^{5 \times 512 \times 512}$, $\tau \in \{1, 2, 3\}$, $x^{\ell,0}$ (today’s PM_{2.5} tile)

Ensure: $\hat{y} = x^{\ell,0} + \Delta$

- 1: Wind sectors $\{s_k\}$ from ERA5 u_{10}, v_{10} over 7×7 groups
- 2: $\mathbf{Z}^g \leftarrow \text{SwinBlocks}(\text{ElevAttn}(\text{UnfoldLinear}(\text{WindShuffle}(\mathbf{x}^g))))$
- 3: $\mathbf{Z}^g \leftarrow \text{WindUnShuffle}(\mathbf{Z}^g)$ ▷ 735×768 , cached once per day
- 4: $\mathbf{Z}^\ell \leftarrow \text{SwinBlocks}(\text{ElevAttn}(\text{UnfoldLinear}(\mathbf{x}^\ell) + \mathbf{E}_{\text{lead}}(\tau)))$
- 5: **for** $i = 1, 2$ **do** ▷ cross-resolution bridge
- 6: $\mathbf{Z}^\ell \leftarrow \mathbf{Z}^\ell + \text{CrossAttn}(\mathbf{Q} = \mathbf{Z}^\ell, \mathbf{KV} = \text{Linear}(\mathbf{Z}^g); \mathbf{B}^{\text{wind}})$
- 7: $\mathbf{Z}^\ell \leftarrow \mathbf{Z}^\ell + \text{FFN}(\mathbf{Z}^\ell)$
- 8: **end for**
- 9: $\Delta \leftarrow \text{PixelShuffleDecoder}(\mathbf{Z}^\ell)$ ▷ zero-init final conv
- 10: **return** $\hat{y} = x^{\ell,0} + \Delta$

The forward pass pseudocode highlights two design choices central to CRAN-PM’s efficiency. First, the Global Branch (lines 1–3) is computed once per forecast day and its output \mathbf{Z}^g is cached and reused across all 126 local tiles. This reduces the total number of global-branch forward passes from $126 \times N_{\text{days}}$ to N_{days} , saving approximately 99% of global-branch computation. Second, the cross-resolution attention (lines 5–7) operates on compressed representations: local queries are $1,024 \times 512$ tokens and global key-values are 735×512 tokens, making the attention matrix $1,024 \times 735 \approx 0.75$ M entries per head, tractable on modern GPUs without approximation. The wind bias \mathbf{B}^{wind} is computed from ERA5 sector assignments and is shared across all cross-attention heads, adding negligible overhead while encoding physical advection direction into every attention computation.